Elsevier Editorial System(tm) for NeuroImage
Manuscript Draft

Manuscript Number: NIMG-13-1336R1

Title: Brain Resting-State Functional MRI Connectivity: Morphological Foundation and Plasticity

Article Type: Regular Article

Section/Category: Anatomy and Physiology

Corresponding Author: Professor Ed X. Wu, PhD

Corresponding Author's Institution: The University of Hong Kong

First Author: Iris Y Zhou, PhD

Order of Authors: Iris Y Zhou, PhD; Yu-Xiang Liang, PhD; Russell W Chan, BEng; Patrick P Gao, BEng; Joe S Cheng, BEng; Yong Hu, PhD; Kwok-Fai So, PhD; Ed X. Wu, PhD

Abstract: Despite the immense ongoing efforts to map brain functional connections and organizations with resting-state functional MRI (rsfMRI), the mechanisms governing the temporally coherent rsfMRI signals remain elusive. In particular, there is a lack of direct evidence regarding the morphological foundation and plasticity of these rsfMRI derived connections. In this study, we investigated the role of axonal projections in rsfMRI connectivity and its plasticity. Well-controlled rodent models of complete and posterior corpus callosotomy were longitudinally examined with rsfMRI at 7 Tesla in conjunction with intracortical EEG recording and functional MRI tracing of interhemispheric neuronal pathways by manganese (Mn^{2+}). At post-callosotomy day 7, significantly decreased interhemispheric rsfMRI connectivity was observed in both groups in the specific cortical areas whose callosal connections were severed. At day 28, the disrupted connectivity was restored in the partial callosotomy group but not in the complete callosotomy group, likely due to the compensation that occurred through the remaining interhemispheric axonal pathways. This restoration - along with the increased intrahemispheric functional connectivity observed in both groups at day 28 - highlight the remarkable adaptation and plasticity in brain rsfMRI connections. These rsfMRI findings were paralleled by the intracortical EEG recording and Mn^{2+} tracing results. Taken together, our experimental results directly demonstrate that axonal connections are the indispensable foundation for rsfMRI connectivity and that such functional connectivity can be plastic and dynamically reorganized atop the morphological connections.

Revision (Clean)

Brain Resting-State Functional MRI Connectivity: Morphological Foundation and Plasticity

Iris Y. Zhou[a,b,1], Yu-Xiang Liang[c,1], Russell W. Chan[a,b], Patrick P. Gao[a,b], Joe S. Cheng[a,b], Yong Hu[d], Kwok-Fai So[c,2], and Ed X. Wu[a,b,c,e,2]

[a]Laboratory of Biomedical Imaging and Signal Processing, [b]Department of Electrical and Electronic Engineering, [c]Department of Anatomy, [d]Department of Orthopaedics and Traumatology, [e]Department of Medicine, The University of Hong Kong, Pokfulam, Hong Kong, China

[1]These authors contribute equally to this work.

[2]Correspondence to:

Prof. Ed X. Wu, Ph.D.
Laboratory of Biomedical Imaging and Signal Processing
Departments of Electrical and Electronic Engineering, Anatomy and Medicine
The University of Hong Kong, Hong Kong SAR, China
Tel: (852) 2859-7096
Fax: (852) 2819-9711
Email: ewu@eee.hku.hk

and Prof. Kwok-Fai So, Ph.D.
Departments of Anatomy
The University of Hong Kong, Hong Kong SAR, China
Tel: (852) 2819-9216

Fax: (852) 2817-0857

Email: hrmaskf@hkucc.hku.hk

Abstract

Despite the immense ongoing efforts to map brain functional connections and organizations with resting-state functional MRI (rsfMRI), the mechanisms governing the temporally coherent rsfMRI signals remain unclear. In particular, there is a lack of direct evidence regarding the morphological foundation and plasticity of these rsfMRI derived connections. In this study, we investigated the role of axonal projections in rsfMRI connectivity and its plasticity. Well-controlled rodent models of complete and posterior corpus callosotomy were longitudinally examined with rsfMRI at 7 Tesla in conjunction with intracortical EEG recording and functional MRI tracing of interhemispheric neuronal pathways by manganese (Mn^{2+}). At post-callosotomy day 7, significantly decreased interhemispheric rsfMRI connectivity was observed in both groups in the specific cortical areas whose callosal connections were severed. At day 28, the disrupted connectivity was restored in the partial callosotomy group but not in the complete callosotomy group, likely due to the compensation that occurred through the remaining interhemispheric axonal pathways. This restoration – along with the increased intrahemispheric functional connectivity observed in both groups at day 28 – highlight the remarkable adaptation and plasticity in brain rsfMRI connections. These rsfMRI findings were paralleled by the intracortical EEG recording and Mn^{2+} tracing results. Taken together, our experimental results directly demonstrate that axonal connections are the indispensable foundation for rsfMRI connectivity and that such functional connectivity can be plastic and dynamically reorganized atop the morphological connections.

Keywords: functional MRI; resting-state network; connectivity; axonal projections; plasticity

Introduction

Since the introduction of blood oxygenation level-dependent (BOLD) contrast (Ogawa et al., 1990), functional MRI (fMRI) has offered a powerful approach for studying brain functions due to its noninvasiveness, large field-of-view and 3D imaging capabilities. Most fMRI studies have focused on examining changes in neuronal activity associated with stimuli or tasks. It is not until recently that there has been immense interest in studying the brain resting-state networks (RSNs) with fMRI. The motivations for such connectivity studies arise mainly from two considerations. First, most of the brain's energy is consumed at rest during spontaneous neuronal activity (20% of body's energy), while task-related increases in energy metabolism are usually small (<5%) (Raichle and Mintun, 2006). Second, spontaneous fluctuations in resting-state fMRI (rsfMRI) signals were found to be temporally coherent among brain areas that are structurally connected and functionally related (Biswal et al., 1995; Fox and Raichle, 2007). This coherence in rsfMRI signals, or so-called functional connectivity, has been widely observed in humans, primates and rodents (Greicius et al., 2003; Lu et al., 2012; Pawela et al., 2008; Vincent et al., 2007). Such phenomena are present in awake brains and persist under anesthesia (Smith et al., 2009; Vincent et al., 2007; Zhang et al., 2010). Functional connectivity, as assessed with rsfMRI, is believed to reflect a rudimentary and intrinsic organization of the resting brain (Fox and Raichle, 2007), and it has been increasingly applied to the study of the complex brain functional networks and their alterations during diseases, aging and learning (Damoiseaux et al., 2008; Jafri et al., 2008; Taubert et al., 2011). Despite rapidly expanding literature in mapping functional connectivity with rsfMRI, the exact biophysical mechanisms

governing the temporally coherent rsfMRI signals remain unclear in the rsfMRI community. In particular, there is a lack of *direct* evidence regarding the morphological foundation and plasticity of resting-state connectivity. Therefore, the precise interpretation of rsfMRI data in both normal and pathological states is hindered.

Considering the similarity between the spatial organization of RSNs and underlying anatomical structures, one view is that functional connectivity is supported by anatomical substrates and that structural connectivity places constraints on the functional interactions occurring at network level. Anatomically, the hemispheres are interconnected by axonal projections through midline commissural structures, such as the corpus callosum (CC), the anterior commissure and the posterior commissure. The largest among these is the CC, which connects most areas of the cerebral cortex to contralateral homologous areas that share similar functions (Kaas, 1995). Considering the primary role of the CC in interhemispheric communication, the role of callosal connections in functional connectivity observed by rsfMRI is naturally an issue of great interest. Two previous human rsfMRI studies on callosal agenesis (Quigley et al., 2003) and complete corpus callosotomy (in a single patient) (Johnston et al., 2008) reported significantly diminished and complete loss of interhemispheric functional connectivity, respectively. These results support structural connections as key constraints on functional connectivity. However, predominately bilateral RSNs have been reported in a patient after complete transection of forebrain commissures (Uddin et al., 2008) and in patients with congenital callosal agenesis (Tyszka et al., 2011). These findings favor another possibility: namely, that functional connectivity can emerge flexibly and exceed the anatomically defined networks. The interpretations of the above studies varied, primarily owing to the lack of

adequate normal controls and complications from pathological conditions. Therefore, the role of the CC in functional connectivity is still open to debate, and the study of well-controlled animal models is valuable in this regard.

Given the primary role of the CC in interconnecting the two hemispheres, the interhemispheric functional connectivity as assessed with rsfMRI may likely originate from intrinsic neural communication mediated by axonal projections through the CC. Furthermore, the RSNs could be innately plastic. Spontaneous fluctuations in rsfMRI signals show strong correlation with intrinsic neuronal activity as measured by electrophysiological recording (Choi et al., 2007). Manganese ion (Mn^{2+}) as a calcium analog has been widely used to visualize functionally specific neuronal pathways *in vivo* due to activity-dependent and axonal tract-tracing Mn^{2+} transport (Chan et al., 2011; Pautler et al., 1998; Silva, 2012; Tucciarone et al., 2009). In this study, we investigated the role of axonal projections in functional connectivity and the plasticity of RSNs. Well-controlled models of complete and partial corpus callosotomy were examined longitudinally with rsfMRI in conjunction with intracortical electroencephalography (EEG) recording and manganese-enhanced MRI (MEMRI) tracing of neuronal connections. Our experimental findings *directly* demonstrate that axonal connections are the indispensable foundation for resting-state functional connectivity and that resting-state networks can be highly plastic atop the morphological connections.

Materials and Methods

Animal Procedures

All experiments were approved by the local institutional animal care and use committee. Adult male Sprague-Dawley rats weighing 220~250 g were divided into three groups and subjected to complete callosotomy (N = 25), posterior partial callosotomy (N = 22) or sham surgery (N = 21). For the surgery, animals were first anesthetized with an intramuscular injection of a mixture of ketamine (80 mg/kg) and xylazine (8 mg/kg). A transection of the entire CC, from bregma +2 mm to -6 mm, was performed on animals in the first group (Ellis-Behnke et al., 2006). Animals in the second group received a transection of the posterior one-third CC, from bregma -3.5 mm to -6 mm. Animals in the sham group had their skulls opened but received no further surgery. Bleeding from the cerebral veins was stopped immediately with cold gel foam, which was removed when homeostasis was satisfactory. After surgery, the animals were returned to their home cages under warm conditions for recovery, and they were housed under a 12:12-hour light/dark cycle in a temperature-controlled room with ad libitum access to food and water. Anti-inflammatory drugs were supplied in the water for one week. Resting-state fMRI was performed on all animals at days 7 and 28 after surgery. At day 30 after surgery, intracortical EEG recordings were performed on 10, 9 and 10 animals from the three groups, respectively. After EEG recording, $MnCl_2$ (100 nl, 500 mM, pH = 7.4) (Sigma-Aldrich, USA), which was dissolved in distilled water, was stereotaxically injected in the locations where EEG recordings were performed, i.e. the right primary somatosensory cortex (S1, bregma +0.2 mm and lateral 3-3.5 mm) and right visual cortex (VC, bregma -7.5 mm and lateral 4 mm), at a rate of 0.01 µl/min with a 1.0 µl Hamilton syringe. The syringe was kept in place for 5 min after injection and then gently removed. The Mn^{2+} concentration was optimized to provide sufficient contrasts for the enhancement of the interhemispheric axonal pathway with minimal injection

volume and neurotoxic effects (Nairismagi et al., 2006; van der Zijden et al., 2007). Manganese-enhanced MRI (MEMRI) was performed 1 day after administration of Mn^{2+}. After all MRI acquisitions, four animals from each group were sacrificed for Luxol fast blue (LFB) staining to examine CC.

MRI Protocols

All MRI measurements were performed utilizing a 7 T Bruker scanner (70/16 PharmaScan, Bruker Biospin GmbH, Germany). The animals were initially anesthetized with 3% isoflurane. When sufficiently anesthetized, 1-2 drops of 2% lidocaine were applied to the chords to provide local anesthesia before the endotracheal intubation. The animals were mechanically ventilated at a rate of 54-56 min^{-1} with 1-1.5% isoflurane in room-temperature air using a ventilator (TOPO, Kent Scientific Corp., Torrington, CT). During MRI, the animals were placed on a plastic cradle with the head fixed with a tooth bar and plastic screws in the ear canals. Rectal temperature was maintained at ~37.0 °C using a water circulation system. Continuous physiological monitoring was performed using an MRI-compatible system (SA Instruments, Stony Brook, NY). Vital signs were within normal physiological ranges (rectal temperature: 36.5–37.5°C, heart rate: 350–420 beat/min, breathing: 54–56 breath/min, oxygen saturation: >95%) throughout the duration of the experiment (Chan et al., 2010; Cheung et al., 2012; Lau et al., 2011; Zhou et al., 2012). Scout T_2-weighted (T2W) images were first acquired to position the subsequent images in a reproducible manner. For rsfMRI, a single-shot gradient-echo echo-planar-imaging (EPI) sequence was used with TR/TE = 1000/18 ms, FOV = 32×32 mm^2, 64×64 matrix, nine 1 mm thick contiguous slices. A total of 420 volumes were collected during each session, and 4-6 sessions were acquired from each animal. RARE T2W images as

anatomical reference for rsfMRI data were acquired at the same locations with TR/TE = 4200/36 ms, 256×256 matrix. To assess and depict CC integrity, diffusion tensor imaging (DTI) was performed in all animals at both post-callosotomy day 7 and 28 using a 4-shot spin-echo EPI sequence with TR/TE = 3000/28.8 ms, δ/Δ = 5/17 ms, 96×96 matrix (zero-filled to 128 × 128) and an encoding scheme of 15 gradient directions at b-value = 1000 s/mm^2 (Hui et al., 2010). For MEMRI, a 3D MP-RAGE sequence was employed to acquire high-resolution volumetric T1-weighted images with TI/TR/TE = 1100/12/4 ms, FOV = 32×32×14 mm^3 and 256×256×28 matrix.

MRI Data Analyses

rsfMRI Analyses

For each rsfMRI session, all images were first corrected for slice timing differences using SPM5 and then realigned to the mean image of the series using 2D rigid-body transformation. The first 20 image volumes of each session were discarded to eliminate possible non-equilibrium effects. A voxel-wise linear detrending with least-squares estimation was performed temporally to eliminate the baseline drift caused by physiological noises and system instability. No spatial smoothing was performed while a temporal band-pass filtering (0.005-0.1 Hz) was applied. Finally, high-resolution T2W images from individual animals were coregistered to T2W images of a reference brain from a normal animal with a 3D rigid-body transformation and the transforming matrix was then applied to the respective rsfMRI data. For independent component analysis (ICA), coregistered rsfMRI data was analyzed with the GIFT v2.0d Toolbox (Hutchison et al., 2010; Jonckers et al., 2011). In brief, the estimated number of components for all rsfMRI data was found to be 37 by the minimum description length (MDL) criterion. The

Infomax algorithm was used and group-level ICA was performed on all rsfMRI data from the same group and at the same time point. The group-level spatial ICA maps of independent resting-state networks (RSNs) were scaled to z-scores with a threshold of $z>2$ (corresponding to a significance level of $p<0.05$). The ICA maps were then visually inspected and labeled based on the spatial patterns in reference to known anatomical and functional locations (Paxinos and Watson, 2005). For seed-based analysis (SBA), functional connectivity was evaluated on a voxel-by-voxel basis (Choi et al., 2007; Pawela et al., 2008). Four cortical areas where bilateral RSNs were commonly observed in the ICA maps of sham animals were examined with SBA. They were secondary somatosensory cortex (S2), primary somatosensory cortex (S1), auditory cortex (AC) and visual cortex (VC). For each brain area, a 2×2-voxel region was chosen as the seed where a high z-score was generally seen in the corresponding ICA maps. Regionally averaged time courses from the voxels within the seed were used as the reference time courses. Pearson's correlation coefficients were calculated between the reference time courses and the time courses of each individual voxel. Correlation coefficients were transformed using Fisher's z transformation and then averaged across runs. The averaged z values were transformed back to correlation coefficients. Subsequently, regions of interest (ROIs) covering the entire left or right parts of the functional areas were defined according to atlas. Mean corrected correlation coefficients (ccc) were obtained by averaging the ccc values within the ROIs.

DTI Analysis

Fractional anisotropy (FA) and color-coded FA maps were calculated by fitting the diffusion tensor model to the diffusion data at each voxel using DTIStudio v3.02 (Chan et al., 2009; Hui et al., 2010).

MEMRI Analysis

MP-RAGE images from each animal were reconstructed three-dimensionally to achieve isotropic voxel size facilitating the identification and visualization of Mn^{2+} transportation. ROIs of VC and S1 were manually defined with reference to the rat brain atlas (Paxinos and Watson, 2005). Signal intensities (SIs) of these ROIs were measured in ImageJ. SIs of the left VC and S1 were normalized to the SIs of the injection sites in the right hemisphere for statistical comparisons between the different groups.

Multi-site EEG Recording and Analysis

At day 30 after surgery, intracortical EEG recording was conducted in animals under 1-1.2% isoflurane anesthesia. Four EEG electrodes (720416 Stainless Steel Metal Macro Electrodes, Harvard Apparatus) were stereotaxically inserted into the cortical regions through four small holes in the skull, located bilaterally at S1 (bregma +0.2 mm and lateral 3-3.5 mm) and VC (bregma -7.5 mm and lateral 4 mm). One electrode was grounded on the animal nose. EEG signals were amplified at a gain of 2,000 and sampled at 10 kHz using National Instruments (Austin, TX) analog/digital card. EEG signals were then band-pass filtered at 0.1–100 Hz and notch-filtered at 50 Hz. Subsequently, the signals were down-sampled to 200 Hz, and a Hilbert transform was applied to quantify the power of the EEG signals. The time courses of EEG power were then truncated into 400-second segments to match the resting-state fMRI data. Pearson's correlation coefficients were calculated to evaluate the EEG power correlation between different electrodes.

Statistical Analysis

For all three types of measurements (ccc values measured by SBA, power correlations of EEG signals and contralateral SI enhancement in MEMRI), statistical comparisons of different groups at the same time point were performed using one-way ANOVA followed by post-hoc testing with Bonferroni correction with $p<0.05$ considered as significant. All *P* values are reported two-tailed. All the results are presented as means ± standard deviations.

Results

Fig. 1 shows the T_2-weighted (T2W) brain images and diffusion fractional anisotropy (FA) maps from the representative Sprague-Dawley rats that had complete callosotomy, posterior partial corpus callosotomy or sham surgery as clearly delineated and confirmed in FA maps. All animals survived after the surgery and animals within each group had similar surgical outcomes. Histological examinations of the animals at post-callosotomy day 31 further confirmed the disruption of callosal connections at the locations of transection (Fig. 2). The rsfMRI data were analyzed using two related but complementary approaches. First, group-level independent component analysis (ICA) was performed for each group, and the resulting spatial maps were matched and compared across groups. Second, seed-based functional connectivity analysis (SBA) was performed, and the regional temporal correlations were compared across groups.

Independent Component Analysis of Functional Connectivity after Corpus Callosotomy

The CC is organized in a rostrocaudal topographical manner, with anterior fibers connecting frontal areas of the two hemispheres and posterior fibers connecting caudal cortical structures. Therefore, to compare the effects of transecting location on different RSNs, four

cortical areas ranging from the anterior to the posterior part of the brain, which correspond to secondary somatosensory cortex (S2), primary somatosensory cortex (S1), auditory cortex (AC) and visual cortex (VC), respectively, were examined. Fig. 3a shows the group-level ICA maps of RSNs corresponding to these areas at post-callosotomy day 7. These components, which cover bilaterally homologous regions in all cortical areas, namely, S2, S1, AC and VC in the sham control animals, were prominently absent in the complete callosotomy group. Instead, two unilateral RSNs were observed for each cortical area. In the partial callosotomy group, where the callosal connections for AC and VC were severed while those for S1 and S2 were largely spared, AC and VC exhibited losses of interhemispheric connectivity while S1 and S2 showed largely preserved connectivity. These ICA findings indicated that callosotomy disrupted interhemispheric functional connectivity in those cortical areas whose primary interhemispheric axonal connections via the CC were severed.

Fig. 3b illustrates the group-level ICA maps of each group at post-callosotomy day 28. Similar to the results observed at post-callosotomy day 7, the complete callosotomy group showed two unilateral RSNs in cortical areas, whereas the sham control group exhibited bilateral components. In contrast, the two unilateral RSNs in AC and VC of the partial callosotomy group observed at post-callosotomy day 7 were no longer seen at post-callosotomy day 28. Instead, AC and VC showed respective RSNs covering bilateral functional homologues that were similar to those of sham controls. These findings indicated that disrupted functional connectivity persisted in the complete callosotomy group but that it was restored in the partial callosotomy group at post-callosotomy day 28.

At post-callosotomy day 28, for animals that underwent complete or partial callosotomy,

the ICA maps exhibited certain spatial expansions of intrahemispheric connectivity in S2 and AC according to visual inspection. Such increased intrahemispheric functional connectivity indicated that the reorganization of RSNs that occurred long after callosotomy might arise from the plasticity of functional brain.

Quantitative Seed-Based Analysis of Functional Connectivity after Corpus Callosotomy

Fig. 4a shows the definitions of seeds and ROIs in S2, S1, AC and VC that were used for SBA. The corrected correlation coefficients (ccc) describing the interhemispheric functional connectivity in different cortical regions of each group at post-callosotomy day 7 and day 28, respectively, are summarized in Fig. 4b. At post-callosotomy day 7, smaller ccc values were generally found in S2, S1, AC and VC in the complete callosotomy group compared to those of sham controls, indicating drastically reduced interhemispheric functional connectivity. Significantly lower ccc values were observed in AC and VC in the posterior partial callosotomy group with respect to sham controls. These quantitative results were in agreement with the ICA results shown in Fig. 3, indicating that interhemispheric functional connectivity was affected in those cortical areas whose callosal connections were severed. At post-callosotomy day 28, significantly lower ccc values were found in all cortical areas in the complete callosotomy group compared to those in sham controls, indicating that the loss of interhemispheric functional connectivity was persistent. However, these significantly smaller ccc values observed in VC and AC in the posterior partial callosotomy group at post-callosotomy day 7 were no longer seen at post-callosotomy day 28. This was consistent with the ICA results, which indicate that restoration of bilateral RSNs in these areas occurred long after partial callosotomy.

EEG Recordings of Inter- and Intrahemispheric Functional Correlations

Resting-state intracortical multi-site EEG recording was performed at post-callosotomy day 30. Power correlation analyses of EEG data within predefined frequency bands were conducted. Fig. 5 summarizes the correlation results from all rats with EEG recordings. In the complete callosotomy group, power correlations between left and right S1 electrode pairs (S1L-S1R) and between left and right VC electrode pairs (VCL-VCR) were significantly lower than those of sham controls in a wide band and were predominantly in low-frequency bands of the delta and theta rhythms. Posterior partial callosotomy severed the callosal connections for VC while sparing those for S1. In parallel, the power correlations of S1L-S1R in the partial callosotomy group were similar to those of the sham controls in all EEG bands examined. Meanwhile, the wide band correlation in VCL-VCR was significantly higher than those in the complete callosotomy group, which was consistent with the rsfMRI findings at day 28, confirming the restoration of interhemispheric functional connectivity in the VC region. Interestingly, VCL-VCR correlations in the partial callosotomy group in the delta band were significantly lower than in the sham controls, and this difference became insignificant in higher-frequency bands (theta, alpha, beta and gamma). This observation suggests that the restoration of interhemispheric connectivity after partial callosotomy might occur in the high-frequency bands, providing insights into the potential mechanisms of the restoration or plasticity from a neural activity perspective.

The power correlation between the right S1 and right VC electrode pairs (S1R-VCR) was generally higher in both callosotomy groups for all EEG bands examined (Fig. 5b). A significant increase in intrahemispheric EEG temporal correlation was observed predominantly – but not exclusively – at lower-frequency bands. Considering that rsfMRI signal correlates with the power

coherence in EEG in the low-frequency bands (Choi et al., 2007), this trend of increased intrahemispheric correlation partly parallel the rsfMRI observation, which likely stemmed from intrahemispheric reorganization after disruption of interhemispheric connectivity.

Functional Mn^{2+} Tracing of Interhemispheric Neuronal Pathways by MEMRI

Mn^{2+} tracing was performed at post-callosotomy day 30 on eight animals from each group after EEG recording to visualize functionally specific neuronal pathways *in vivo* due to the activity-dependent and axonal tract-tracing Mn^{2+} transport. Fig. 6a shows the interhemispheric S1 and VC connections revealed by Mn^{2+} tracing at post-callosotomy day 30. In the complete callosotomy group, no significant contralateral enhancement was observed for S1 or VC. Meanwhile, robust contralateral Mn^{2+} enhancement in S1 in the partial callosotomy group and in S1 and VC in the sham controls (arrowheads) indicated their normal interhemispheric neuronal connections. More importantly, a moderate contralateral enhancement in VC in the partial callosotomy group revealed the availability or presence of interhemispheric neuronal pathway for VC long after the corresponding callosal connections were severed. The restoration of such neuronal pathway most likely occurred at the axonal level because the long-range Mn^{2+} transport to the contralateral homologues was predominantly via the interhemispheric callosal route. Normalized contralateral Mn^{2+} enhancement in terms of signal intensity (SI) was compared in different groups and is shown in Fig. 6b.

Interhemispheric Connectivity after Corpus Callosotomy: rsfMRI vs. EEG vs. MEMRI

Fig. 7 compares interhemispheric connectivity in S1 and VC as measured by SBA of rsfMRI, power correlations of EEG and contralateral enhancement in MEMRI for animals examined by

the three methods, at the chronic stage of callosotomy. Similar trends in group differences were revealed by all three methods (Fig. 7a). In addition, rsfMRI, EEG and MEMRI measurements in S1 and VC in those individual animals that underwent all three examinations are also depicted in three-dimensional scatter plots (Fig. 7b). As clearly seen from the scatter plots, for S1, the complete callosotomy group forms a cluster closer to the origin and separates from the overlapping plots of the other two groups. For VC, clusters of different groups are well separated. Pearson's correlation coefficients (r) were calculated using the results from all the individual animals from the three groups (N=24) to quantify the correlation between any two measurements. In S1, the r values were 0.41 (p=0.047, rsfMRI vs. EEG), 0.50 (p=0.013, rsfMRI vs. MEMRI) and 0.59 (p=0.002, EEG vs. MEMRI), respectively. In VC, the r values were 0.63 (p=0.001, rsfMRI vs. EEG), 0.50 (p=0.013, rsfMRI vs. MEMRI) and 0.64 (p=0.001, EEG vs. MEMRI), respectively. Therefore, all three independent measurements from individual animals exhibit positive correlations. In other words, the rsfMRI findings of the persistent loss of interhemispheric functional connectivity in S1 and VC of complete callosotomy group and the restoration of bilateral RSNs in VC of partial callosotomy group long after callosotomy surgery were paralleled by the intracortical EEG recording and Mn^{2+} tracing results.

Discussion

In this study, well-controlled experimental models of corpus callosotomy were employed to investigate the role of axonal or structural connections in functional connectivity measured by rsfMRI and the plasticity of RSNs. Complete callosotomy resulted in a loss of

interhemispheric functional connectivity in all cortical areas examined at both day 7 and day 28. For partial callosotomy, significantly decreased interhemispheric functional connectivity was noted at day 7 in those cortical areas whose primary interhemispheric connections via the CC were severed. However, this disrupted connectivity was restored at day 28. Furthermore, intrahemispheric functional connectivity was generally found to increase at day 28. Using *in vivo* multi-site EEG recording at day 30, similar findings to rsfMRI results of day 28 were observed. Functional neuronal tracing by local Mn^{2+} injection at day 30 also showed that interhemispheric Mn^{2+} transport was absent in areas exhibiting functional connectivity loss but was present in areas exhibiting normal or restored functional connectivity in rsfMRI and EEG. Moreover, strong positive correlations were found between the independent rsfMRI, EEG and MEMRI measurements long after callosotomy surgery in those individual animals that underwent all three examinations.

The Role of Callosal Connections in Interhemispheric Functional Connectivity

Though our understanding of the brain intrinsic activity is expanding rapidly, the neurophysiological mechanisms underlying functional networks measured by rsfMRI and their relationship to morphological or structural networks are not fully understood. Given the similarity between the spatial patterns of coherence in rsfMRI signals and anatomically defined networks, one view is that functional connectivity is organized on the basis of structural connections. Early EEG studies showed decreased interhemispheric coherence in patients after corpus callosotomy or with callosal agenesis (Matsuzaka et al., 1993; Montplaisir et al., 1990; Nielsen et al., 1993). Recently, a case study in a 6-year-old child before and after complete corpus callosotomy for the treatment of intractable epilepsy showed a loss of interhemispheric

functional connectivity in rsfMRI with preserved intrahemispheric functional connectivity (Johnston et al., 2008). Another study reported significantly reduced interhemispheric functional connectivity in motor and auditory cortices in three patients with callosal agenesis (Quigley et al., 2003). These findings suggest that the absence of callosal connections could lead to diminished interhemispheric functional connectivity, indicating the essential role of the CC in functional connectivity. In addition, studies using rsfMRI in combination with diffusion MRI have demonstrated that functional connectivity and structural connectivity are strongly correlated (Bullmore and Sporns, 2009; Greicius et al., 2009; Honey et al., 2009). More recently, a simulation study revealed that structural disconnection would induce the same qualitative changes in resting-state brain activity (Cabral et al., 2012). All of these findings support the fundamental role of structural connections in functional connectivity (Cabral et al., 2012). However, one early EEG study showed no substantial difference in the interhemispheric correlation between an epileptic patient with partial callosotomy and matched controls (Corsi-Cabrera et al., 1995). A recent rsfMRI report noted the presence of bilateral networks in an epileptic patient 45 years after complete transection of the forebrain commissures (Uddin et al., 2008). Moreover, predominately bilateral symmetric resting-state networks were observed in a group of people with congenital callosal agenesis (Tyszka et al., 2011). All of these results indicate that the absence of major axonal or structural connections does not preclude resting-state connectivity. However, the possibility that resting-state networks may be restored or compensated through other structural connections could not be excluded from these interpretations.

In this study, we examined the functional connectivity changes in normal adult brains after

complete and partial corpus callosotomy. This approach enabled us to access direct evidence for the role of callosal/axonal connection in the genesis of functional connectivity without interference from development, epilepsy or medication conditions. ICA was employed to determine the spatial distribution of resting-state networks, while seed-based analysis (SBA) was used to determine the functional connectivity quantitatively. As shown in Figs. 3 and 4, both ICA and SBA results demonstrated a striking loss of interhemispheric correlations in the cortical areas after complete corpus callosotomy at post-callosotomy day 7, indicating the essential role of callosal connections in functional connectivity. All of the cortical areas examined in this study, namely, S2, S1, AC and VC, send axonal projections to their contralateral homologues via different sections of the CC (Jouandet et al., 1986; Lomber et al., 1994; Nakamura and Kanaseki, 1989; Olavarria and van Sluyters, 1986). For example, S1 sends callosal projections to the contralateral cortex via the midbody of the CC, while axonal fibers from the VC are confined to the posterior section of the CC and the splenium. In this study, animals with posterior partial callosotomy exhibited losses of functional connectivity at post-callosotomy day 7 in AC and VC whose corresponding callosal fibers were transected. Our findings revealed the strong dependence of resting-state networks on their callosal connections, directly validating the crucial role of structural connections.

Plasticity in Inter- and Intrahemispheric Functional Connectivity after Callosotomy

At 28 days after the partial callosotomy, the bilateral ICA components were restored in AC and VC in the posterior partial callosotomy group (Fig. 3). The corresponding ccc value was comparable to that of the sham control (Fig. 4). These results indicated that the disrupted interhemispheric functional connectivity in the partial callosotomy groups had recovered, at

least partially, at the chronic stage of callosotomy. Recently, a pediatric case study also reported the restoration of bilateral resting-state networks after partial corpus callosotomy (Pizoli et al., 2011). The recovery of resting-state networks has also been reported after stroke (van Meer et al., 2012). One explanation was that the compensation could occur through the interhemispheric axonal pathways crossing the remaining CC, as the restoration was observed only in the partial corpus callosotomy group where the activity-driven Mn^{2+} transport via interhemispheric axonal route was also detected. Our findings here indicate that, while structural connections are the indispensable framework for functional connectivity, the latter could be mediated or modified by activities over the former.

Increased intrahemispheric functional connectivity was generally found in all the observed cortical areas in the animals with partial or complete callosotomy. In this study of callosotomy in adult rat brains, extensive structural reorganization may not take place as has been observed in the developing brain (Moumdjian et al., 1991). An early study using a horseradish peroxidase technique reported that the overall pattern of intrahemispheric anatomical connections in the brains of mice with congenital callosal agenesis was not different from that of normal mice (Ozaki et al., 1989). Therefore, the increased intrahemispheric functional connectivity observed in this study likely arose from the activity-induced functional alterations or reorganization.

Future Work

The neurophysiological mechanisms of resting-state neuronal activities, their spatiotemporal organization and plasticity are undoubtedly complex. The compensatory activities occurring at functional network level, as observed in this study, remain to be elucidated in the future. In addition, animal models of corpus callosotomy could be further

pursued in the following directions. First, detailed assessment of the behavioral changes following various extents of corpus callosotomy is desired though, in this study, no apparent behavioral differences among the complete, partial and sham callosotomy groups were observed at day 7 and day 28 after surgery. Recent studies suggest the crucial role of spontaneous activity in mediating behavioral responses by providing top-down modulation of sensory processing (Boly et al., 2007; Dubovik et al., 2012). Therefore, future study of the relationship between behavior changes and connectivity alterations after callosotomy may provide new insights into the causal relationship between brain connectivity and functions. Second, the interhemispheric vasculature network around the CC could have been unavoidably damaged during the callosotomy in this study. Such vascular change might affect the local and global BOLD signals, thus could potentially influence the functional connectivity measured by rsfMRI. Nevertheless, EEG recording is considered as a pure measurement of neuronal activity without confounding factors from the hemodynamic response that is associated with BOLD signals. Our EEG experiments returned similar results as those observed from rsfMRI. Considering the strong correlation between spontaneous fluctuations in rsfMRI and EEG oscillations (Wang et al., 2012), the effects of vascular damage likely would not affect or dominate the interhemispheric rsfMRI connectivity loss or the RSN plasticity observed in this study. Lastly, recent studies suggests that the thalamus, as the sensory switchboard, may also mediate bilateral synchronization of cortical activities (Sherman, 2007). Subcortical regions, which are not predominately interconnected by callosal connections, were not expected to be significantly affected by the callosotomy. In this study, bilateral RSNs in thalamus, hippocampus and striatum could be still observed from most animals from all groups. Given the

cortico-thalamic and cortico-striatal connections as essential pathways in the brain, the thalamus and basal ganglia might play certain roles in the RSN plasticity observed in the present study, which is an issue to be explored in the future.

Conclusion

In conclusion, at post-callosotomy day 7, significantly decreased interhemispheric connectivity was observed in multiple cortical areas with severed callosal connections in both the complete and partial callosotomy groups, indicating an indispensable role for axonal connections via the CC in functional connectivity. At day 28, this disrupted functional connectivity was at least partially restored in the partial callosotomy group, but not in the complete callosotomy group. This restoration, along with the increased intrahemispheric functional connectivity found in both callosotomy groups at day 28, demonstrates the remarkable adaptation and plasticity of RSNs. These rsfMRI findings were supported by the interhemispheric EEG coherence results. Furthermore, functional neuronal tracing by local Mn^{2+} injection showed that interhemispheric Mn^{2+} transport was absent in areas exhibiting functional connectivity loss but was present in areas exhibiting normal or restored functional connectivity in rsfMRI and EEG. Taken together, these experimental findings underscore the essential role of axonal connections in rsfMRI and, more importantly, demonstrate the plasticity of RSNs. They *directly* support that axonal projections are the indispensable framework for functional connectivity and that functional connectivity can be dynamically reorganized atop the morphological connections.

Acknowledgements

This work was supported in part by Hong Kong Research Grants Council (General Research Grants HKU7808/09M, HKU7826/10M and HKU7837/11M to E.X.W.)

References

Biswal, B., Yetkin, F.Z., Haughton, V.M., Hyde, J.S., 1995. Functional connectivity in the motor cortex of resting human brain using echo-planar MRI. Magn Reson Med 34, 537-541.

Boly, M., Balteau, E., Schnakers, C., Degueldre, C., Moonen, G., Luxen, A., Phillips, C., Peigneux, P., Maquet, P., Laureys, S., 2007. Baseline brain activity fluctuations predict somatosensory perception in humans. Proc Natl Acad Sci U S A 104, 12187-12192.

Bullmore, E., Sporns, O., 2009. Complex brain networks: graph theoretical analysis of structural and functional systems. Nat Rev Neurosci 10, 186-198.

Cabral, J., Hugues, E., Kringelbach, M.L., Deco, G., 2012. Modeling the outcome of structural disconnection on resting-state functional connectivity. Neuroimage 62, 1342-1353.

Chan, K.C., Khong, P.L., Cheung, M.M., Wang, S., Cai, K.X., Wu, E.X., 2009. MRI of late microstructural and metabolic alterations in radiation-induced brain injuries. J Magn Reson Imaging 29, 1013-1020.

Chan, K.C., Li, J., Kau, P., Zhou, I.Y., Cheung, M.M., Lau, C., Yang, J., So, K.F., Wu, E.X., 2011. In vivo retinotopic mapping of superior colliculus using manganese-enhanced magnetic resonance imaging. Neuroimage 54, 389-395.

Chan, K.C., Xing, K.K., Cheung, M.M., Zhou, I.Y., Wu, E.X., 2010. Functional MRI of postnatal visual development

in normal and hypoxic-ischemic-injured superior colliculi. Neuroimage 49, 2013-2020.

Cheung, M.M., Lau, C., Zhou, I.Y., Chan, K.C., Zhang, J.W., Fan, S.J., Wu, E.X., 2012. High fidelity tonotopic mapping using swept source functional magnetic resonance imaging. Neuroimage 61, 978-986.

Choi, J.K., Dedeoglu, A., Jenkins, B.G., 2007. Application of MRS to mouse models of neurodegenerative illness. NMR in Biomedicine 20, 216-237.

Corsi-Cabrera, M., Trias, G., Guevara, M.A., Haro, R., Hernandez, A., 1995. EEG interhemispheric correlation after callosotomy: one case study. Percept Mot Skills 80, 504-506.

Damoiseaux, J.S., Beckmann, C.F., Arigita, E.J., Barkhof, F., Scheltens, P., Stam, C.J., Smith, S.M., Rombouts, S.A., 2008. Reduced resting-state brain activity in the "default network" in normal aging. Cereb Cortex 18, 1856-1864.

Dubovik, S., Pignat, J.M., Ptak, R., Aboulafia, T., Allet, L., Gillabert, N., Magnin, C., Albert, F., Momjian-Mayor, I., Nahum, L., Lascano, A.M., Michel, C.M., Schnider, A., Guggisberg, A.G., 2012. The behavioral significance of coherent resting-state oscillations after stroke. Neuroimage.

Ellis-Behnke, R.G., Liang, Y.X., You, S.W., Tay, D.K., Zhang, S., So, K.F., Schneider, G.E., 2006. Nano neuro knitting: peptide nanofiber scaffold for brain repair and axon regeneration with functional return of vision. Proc Natl Acad Sci U S A 103, 5054-5059.

Fox, M.D., Raichle, M.E., 2007. Spontaneous fluctuations in brain activity observed with functional magnetic resonance imaging. Nat Rev Neurosci 8, 700-711.

Greicius, M.D., Krasnow, B., Reiss, A.L., Menon, V., 2003. Functional connectivity in the resting brain: a network analysis of the default mode hypothesis. Proc Natl Acad Sci U S A 100, 253-258.

Greicius, M.D., Supekar, K., Menon, V., Dougherty, R.F., 2009. Resting-state functional connectivity reflects structural connectivity in the default mode network. Cereb Cortex 19, 72-78.

Honey, C.J., Sporns, O., Cammoun, L., Gigandet, X., Thiran, J.P., Meuli, R., Hagmann, P., 2009. Predicting human resting-state functional connectivity from structural connectivity. Proc Natl Acad Sci U S A 106, 2035-2040.

Hui, E.S., Cheung, M.M., Chan, K.C., Wu, E.X., 2010. B-value dependence of DTI quantitation and sensitivity in detecting neural tissue changes. Neuroimage 49, 2366-2374.

Hutchison, R.M., Mirsattari, S.M., Jones, C.K., Gati, J.S., Leung, L.S., 2010. Functional networks in the anesthetized rat brain revealed by independent component analysis of resting-state FMRI. J Neurophysiol 103, 3398-3406.

Jafri, M.J., Pearlson, G.D., Stevens, M., Calhoun, V.D., 2008. A method for functional network connectivity among spatially independent resting-state components in schizophrenia. Neuroimage 39, 1666-1681.

Johnston, J.M., Vaishnavi, S.N., Smyth, M.D., Zhang, D., He, B.J., Zempel, J.M., Shimony, J.S., Snyder, A.Z., Raichle, M.E., 2008. Loss of resting interhemispheric functional connectivity after complete section of the corpus callosum. J Neurosci 28, 6453-6458.

Jonckers, E., Van Audekerke, J., De Visscher, G., Van der Linden, A., Verhoye, M., 2011. Functional connectivity fMRI of the rodent brain: comparison of functional connectivity networks in rat and mouse. PLoS One 6, e18876.

Jouandet, M.L., Lachat, J.J., Garey, L.J., 1986. Topographic distribution of callosal neurons and terminals in the cerebral cortex of the cat. Anat Embryol (Berl) 173, 323-342.

Kaas, J.H., 1995. The organization of callosal connections in primates. In: Reeves, A.G., Roberts, D.W. (Eds.), Epilepsy and the Corpus Callosum 2. Advances in behavioral biology. Plenum Press, New York, pp. 15-27.

Lau, C., Zhang, J.W., Xing, K.K., Zhou, I.Y., Cheung, M.M., Chan, K.C., Wu, E.X., 2011. BOLD responses in the superior colliculus and lateral geniculate nucleus of the rat viewing an apparent motion stimulus. Neuroimage 58, 878-884.

Lomber, S.G., Payne, B.R., Rosenquist, A.C., 1994. The spatial relationship between the cerebral cortex and fiber

trajectory through the corpus callosum of the cat. Behav Brain Res 64, 25-35.

Lu, H., Zou, Q., Gu, H., Raichle, M.E., Stein, E.A., Yang, Y., 2012. Rat brains also have a default mode network. Proc Natl Acad Sci U S A 109, 3979-3984.

Matsuzaka, T., Ono, K., Baba, H., Matsuo, M., Tanaka, S., Tsuji, Y., Sugai, S., 1993. Interhemispheric correlation analysis of EEGs before and after corpus callosotomy. Jpn J Psychiatry Neurol 47, 329-330.

Montplaisir, J., Nielsen, T., Cote, J., Boivin, D., Rouleau, I., Lapierre, G., 1990. Interhemispheric EEG coherence before and after partial callosotomy. Clin Electroencephalogr 21, 42-47.

Moumdjian, R.A., Antel, J.P., Yong, V.W., 1991. Origin of contralateral reactive gliosis in surgically injured rat cerebral cortex. Brain Res 547, 223-228.

Nairismagi, J., Pitkanen, A., Narkilahti, S., Huttunen, J., Kauppinen, R.A., Grohn, O.H., 2006. Manganese-enhanced magnetic resonance imaging of mossy fiber plasticity in vivo. Neuroimage 30, 130-135.

Nakamura, H., Kanaseki, T., 1989. Topography of the corpus callosum in the cat. Brain Res 485, 171-175.

Nielsen, T., Montplaisir, J., Lassonde, M., 1993. Decreased interhemispheric EEG coherence during sleep in agenesis of the corpus callosum. Eur Neurol 33, 173-176.

Ogawa, S., Lee, T.M., Nayak, A.S., Glynn, P., 1990. Oxygenation-sensitive contrast in magnetic resonance image of rodent brain at high magnetic fields. Magn Reson Med 14, 68-78.

Olavarria, J., van Sluyters, R.C., 1986. Axons from restricted regions of the cortex pass through restricted portions of the corpus callosum in adult and neonatal rats. Brain Res 390, 309-313.

Ozaki, H.S., Iwahashi, K., Shimada, M., 1989. Ipsilateral corticocortical projections of fibers which course within Probst's longitudinal bundle seen in the brains of mice with congenital absence of the corpus callosum: a study with the horseradish peroxidase technique. Brain Res 493, 66-73.

Pautler, R.G., Silva, A.C., Koretsky, A.P., 1998. In vivo neuronal tract tracing using manganese-enhanced magnetic resonance imaging. Magn Reson Med 40, 740-748.

Pawela, C.P., Biswal, B.B., Cho, Y.R., Kao, D.S., Li, R., Jones, S.R., Schulte, M.L., Matloub, H.S., Hudetz, A.G., Hyde, J.S., 2008. Resting-state functional connectivity of the rat brain. Magn Reson Med 59, 1021-1029.

Paxinos, G., Watson, C., 2005. The rat brain in stereotaxic coordinates. Elsevier Academic Press.

Pizoli, C.E., Shah, M.N., Snyder, A.Z., Shimony, J.S., Limbrick, D.D., Raichle, M.E., Schlaggar, B.L., Smyth, M.D., 2011. Resting-state activity in development and maintenance of normal brain function. Proc Natl Acad Sci U S A 108, 11638-11643.

Quigley, M., Cordes, D., Turski, P., Moritz, C., Haughton, V., Seth, R., Meyerand, M.E., 2003. Role of the corpus callosum in functional connectivity. AJNR Am J Neuroradiol 24, 208-212.

Raichle, M.E., Mintun, M.A., 2006. Brain work and brain imaging. Annu Rev Neurosci 29, 449-476.

Sherman, S.M., 2007. The thalamus is more than just a relay. Curr Opin Neurobiol 17, 417-422.

Silva, A.C., 2012. Using manganese-enhanced MRI to understand BOLD. Neuroimage 62, 1009-1013.

Smith, S.M., Fox, P.T., Miller, K.L., Glahn, D.C., Fox, P.M., Mackay, C.E., Filippini, N., Watkins, K.E., Toro, R., Laird, A.R., Beckmann, C.F., 2009. Correspondence of the brain's functional architecture during activation and rest. Proc Natl Acad Sci U S A 106, 13040-13045.

Taubert, M., Lohmann, G., Margulies, D.S., Villringer, A., Ragert, P., 2011. Long-term effects of motor training on resting-state networks and underlying brain structure. Neuroimage 57, 1492-1498.

Tucciarone, J., Chuang, K.H., Dodd, S.J., Silva, A., Pelled, G., Koretsky, A.P., 2009. Layer specific tracing of corticocortical and thalamocortical connectivity in the rodent using manganese enhanced MRI. Neuroimage 44, 923-931.

Tyszka, J.M., Kennedy, D.P., Adolphs, R., Paul, L.K., 2011. Intact bilateral resting-state networks in the absence of the corpus callosum. J Neurosci 31, 15154-15162.

Uddin, L.Q., Mooshagian, E., Zaidel, E., Scheres, A., Margulies, D.S., Kelly, A.M., Shehzad, Z., Adelstein, J.S., Castellanos, F.X., Biswal, B.B., Milham, M.P., 2008. Residual functional connectivity in the split-brain revealed with resting-state functional MRI. Neuroreport 19, 703-709.

van der Zijden, J.P., Wu, O., van der Toorn, A., Roeling, T.P., Bleys, R.L., Dijkhuizen, R.M., 2007. Changes in neuronal connectivity after stroke in rats as studied by serial manganese-enhanced MRI. Neuroimage 34, 1650-1657.

van Meer, M.P., Otte, W.M., van der Marel, K., Nijboer, C.H., Kavelaars, A., van der Sprenkel, J.W., Viergever, M.A., Dijkhuizen, R.M., 2012. Extent of bilateral neuronal network reorganization and functional recovery in relation to stroke severity. J Neurosci 32, 4495-4507.

Vincent, J.L., Patel, G.H., Fox, M.D., Snyder, A.Z., Baker, J.T., Van Essen, D.C., Zempel, J.M., Snyder, L.H., Corbetta, M., Raichle, M.E., 2007. Intrinsic functional architecture in the anaesthetized monkey brain. Nature 447, 83-86.

Wang, L., Saalmann, Y.B., Pinsk, M.A., Arcaro, M.J., Kastner, S., 2012. Electrophysiological low-frequency coherence and cross-frequency coupling contribute to BOLD connectivity. Neuron 76, 1010-1020.

Zhang, N., Rane, P., Huang, W., Liang, Z., Kennedy, D., Frazier, J.A., King, J., 2010. Mapping resting-state brain networks in conscious animals. J Neurosci Methods 189, 186-196.

Zhou, I.Y., Cheung, M.M., Lau, C., Chan, K.C., Wu, E.X., 2012. Balanced steady-state free precession fMRI with intravascular susceptibility contrast agent. Magn Reson Med 68, 65-73.

Figure Legends

Fig. 1 Typical T_2-weighted (T2W) images and fractional anisotropy (FA) maps from the animals with complete (**a**), posterior partial (**b**) corpus callosotomy and sham surgery (**c**), at day 7 after surgery. The transected part of the corpus callosum (CC) is indicated in red in the sagittal planes (left panel) and with yellow arrows in the T2W and FA images. The drastic FA reduction confirms axonal fiber disruption or callosotomy. The blue lines in the left panel indicate the corresponding locations of T2W and FA slices in the right panel.

Fig. 2 Typical Luxol fast blue (LFB)-stained sections from the animals with complete, posterior partial corpus callosotomy and sham surgery. LFB staining performed at post-callosotomy day 30 confirmed the disruption of callosal connections at the locations of transection. The transected part of the CC is indicated by yellow arrows.

Fig. 3 Functional connectivity maps from animal groups with complete, posterior partial callosotomy and sham surgery at post-surgery day 7 (**a**) and day 28 (**b**). Spatial ICA maps of independent components were scaled to z-scores ($z>2$) and overlaid on a T_2-weighted anatomical template. The color bars display z-scores, with a higher z-score representing a stronger correlation between the time course of that voxel and the mean time course of the component. The components shown in this figure correspond to four cortical areas ranging from the anterior to posterior part of the brain. They are the secondary somatosensory cortex (S2), primary somatosensory cortex (S1), auditory cortex (AC) and visual cortex (VC), respectively.

Fig. 4 The seeds and corresponding regions of interest (ROIs) for seed-based analysis (SBA) are defined based on the ICA connectivity results (**a**). They are overlaid on EPI images. Corrected correlation coefficients calculated between the rsfMRI time courses of the seeds and the

contralateral ROIs quantitatively measure the interhemispheric functional connectivity at post-callosotomy days 7 and 28 (**b**). The results are presented as means ± standard deviations. Statistical comparisons between different groups were performed using one-way ANOVA followed by post-hoc testing with Bonferroni correction with *p<0.05, **p<0.01, ***p<0.005.

Fig. 5 Power correlation analysis interhemispherically (**a**) and intrahemispherically (**b**) from intracortical EEG recordings at post-callosotomy day 30. The powers of the wide, delta, theta, alpha, beta and gamma bands were extracted, and their correlations were calculated between the left and right S1 regions (S1L-S1R), between the left and right VC regions (VCL-VCR) and between the right S1 and right VC regions (S1R-VCR). Error bars represent standard deviations. Statistical comparisons between different groups were performed using one-way ANOVA followed by post-hoc testing with Bonferroni correction with *p<0.05, **p<0.01, ***p<0.005.

Fig. 6 Mn^{2+} tracing was performed on eight animals from each group after EEG recording at post-callosotomy day 30 to visualize interhemispheric neuronal pathways with activity-dependent and axonal tract-tracing Mn^{2+} transport using MEMRI (**a**). Mn^{2+}-induced enhancement in the contralateral S1 and VC was evaluated by the signal intensity of the contralateral side normalized by that of the ipsilateral side (**b**). Error bars represent standard deviations. Statistical comparisons between different groups were performed using one-way ANOVA followed by post-hoc testing with Bonferroni correction with **p<0.01, ***p<0.005.

Fig. 7 The interhemispheric connectivity in S1 and VC as measured by SBA of rsfMRI at post-callosotomy day 28, the power correlations of EEG recording at post-callosotomy day 30 and contralateral enhancement in MEMRI performed at post-callosotomy day 31 for each group were plotted together for comparison (**a**). In addition, rsfMRI, EEG and MEMRI measurements in S1 and VC of those individual animals examined by all three methods are shown in three-dimensional scatter plots (**b**).

Figure 1

Click here to download high resolution image

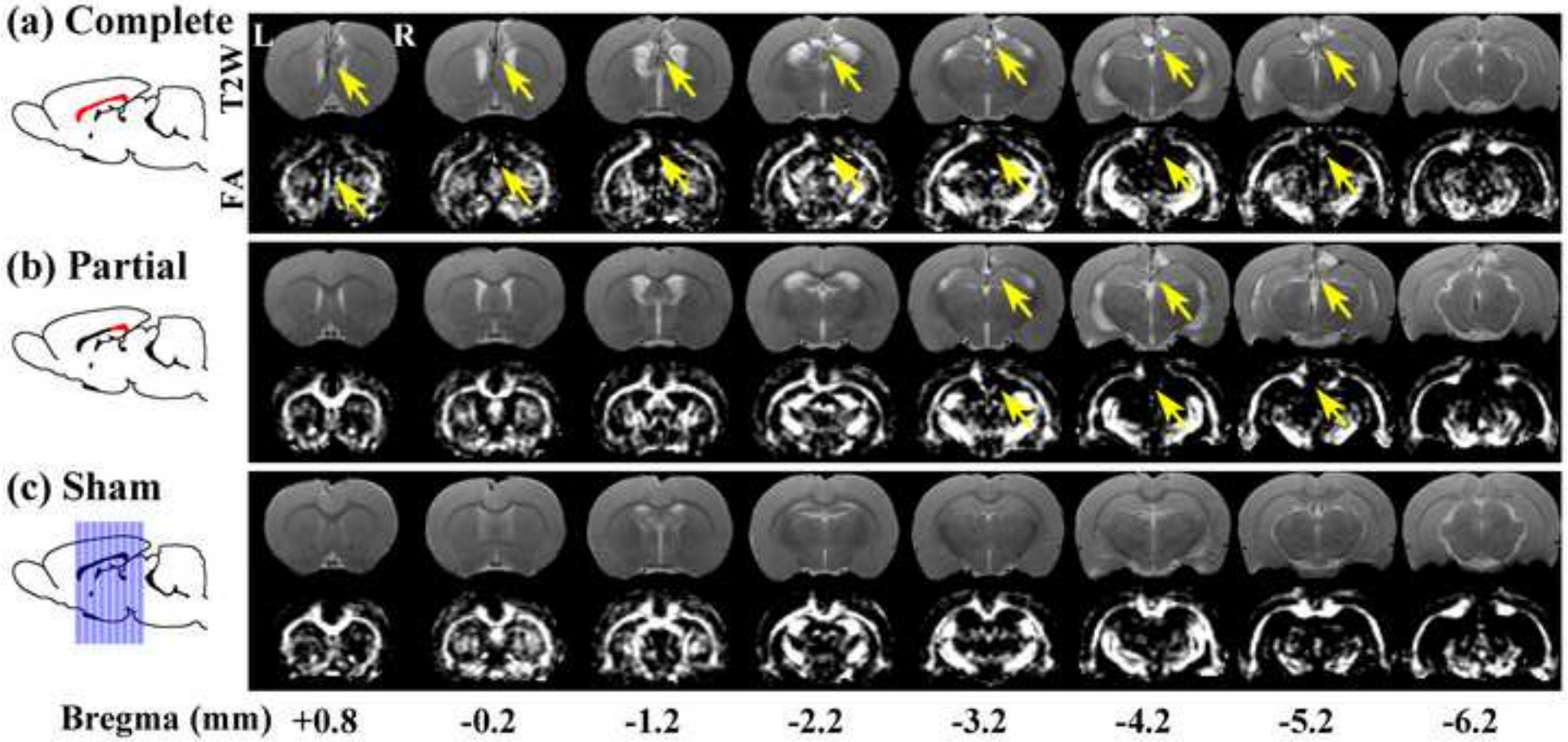

Figure 2

Click here to download high resolution image

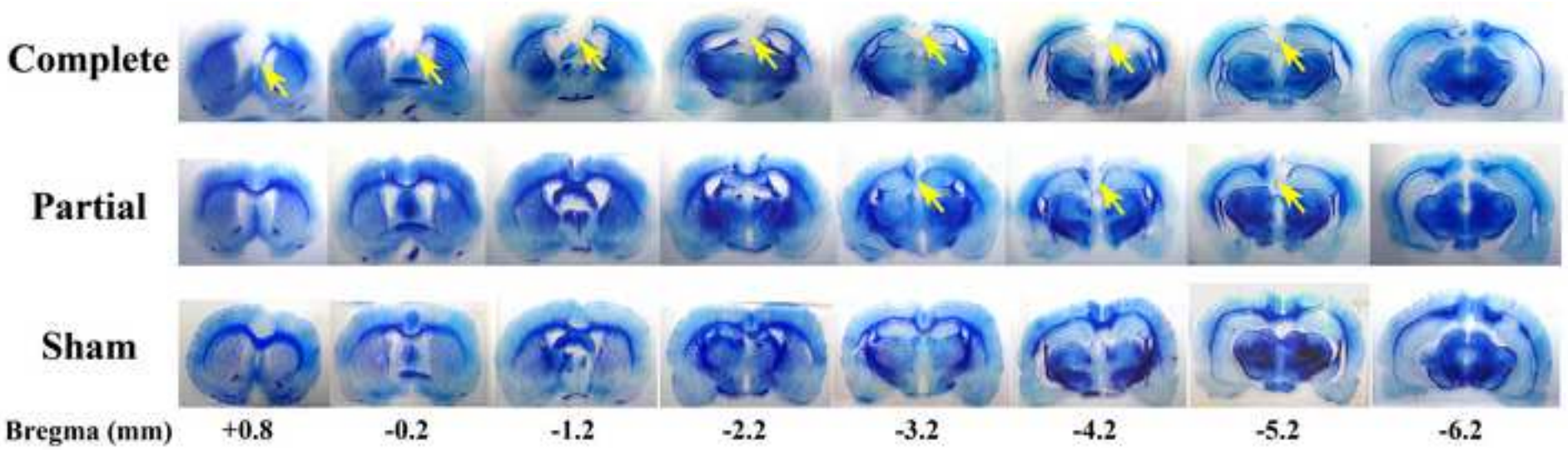

Figure 3

Click here to download high resolution image

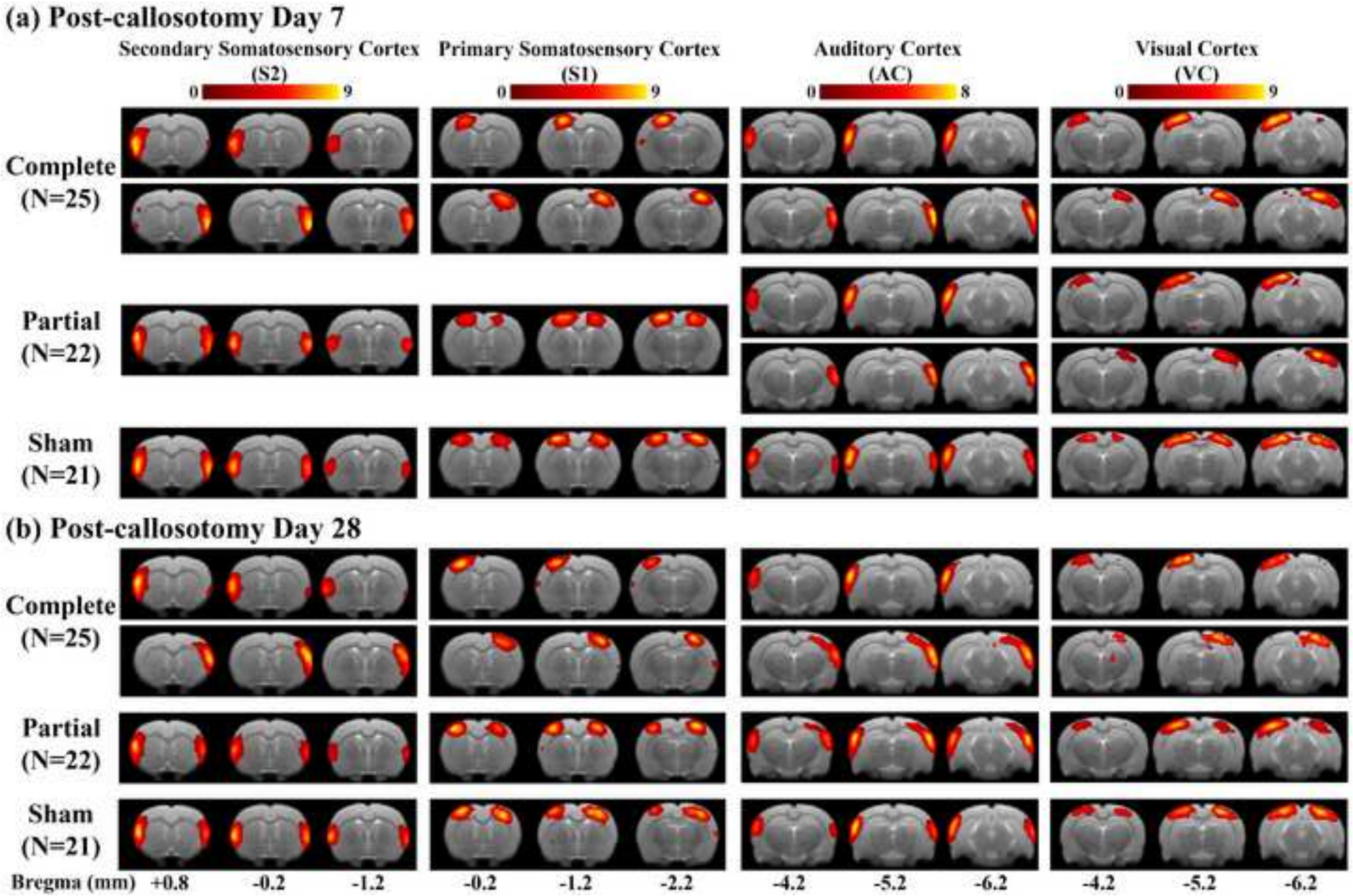

Figure 4

Click here to download high resolution image

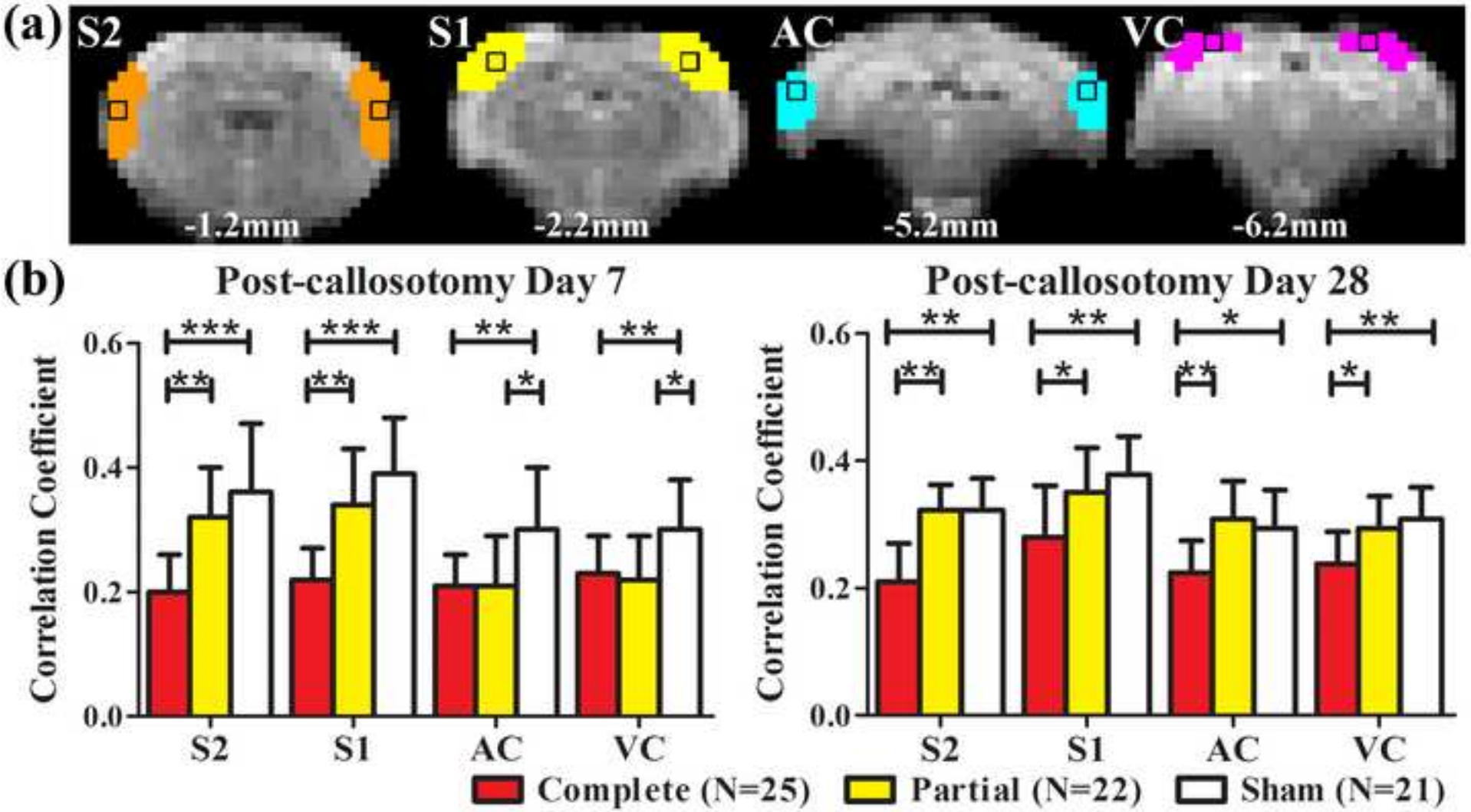

Figure 5

Click here to download high resolution image

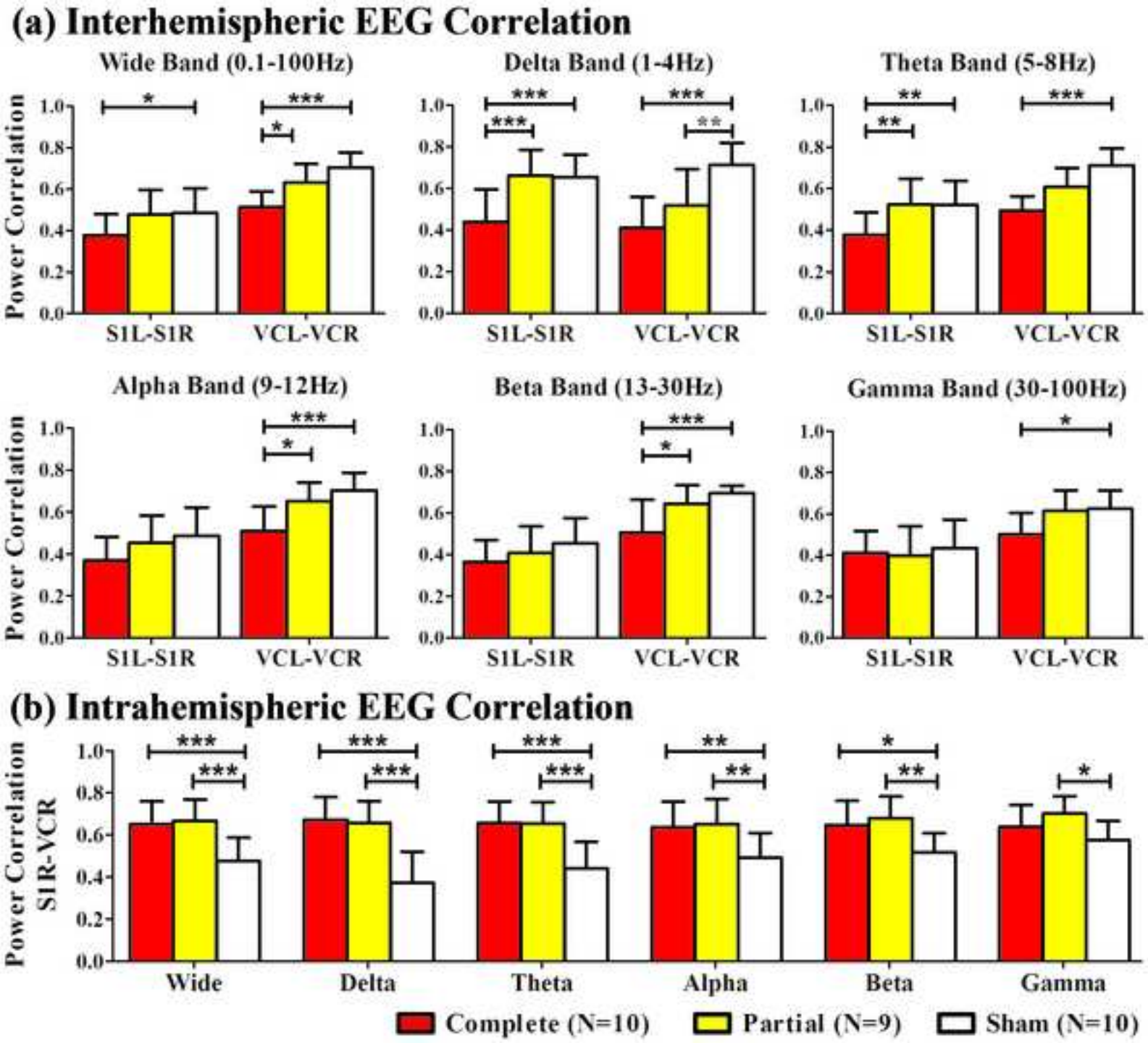

Figure 6

Click here to download high resolution image

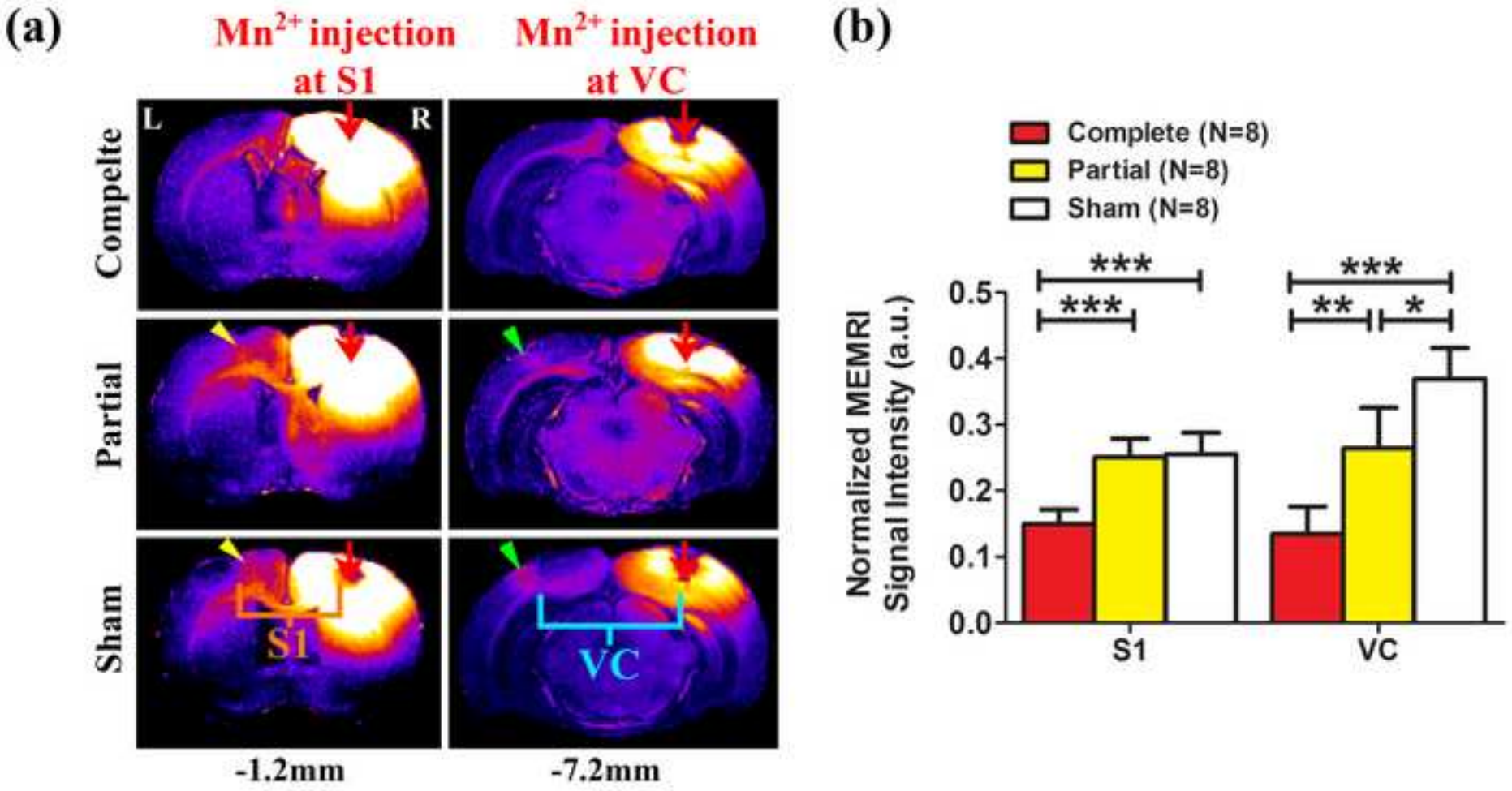

Figure 7

Click here to download high resolution image